JACS
JOURNAL OF THE AMERICAN CHEMICAL SOCIETY
Article
pubs.acs.org/JACS

Periodic Grain Boundaries Formed by Thermal Reconstruction of Polycrystalline Graphene Film

Bao Yang, Hai Xu, Jiong Lu, and Kian Ping Loh*

Department of Chemistry and Graphene Research Centre, National University of Singapore, 3 Science Drive 3, Singapore 117543

Supporting Information

ABSTRACT: Grain boundaries consisting of dislocation cores arranged in a periodic manner have well-defined structures and peculiar properties and can be potentially applied as conducting circuits, plasmon reflectors and phase retarders. Pentagon-heptagon (5−7) pairs or pentagon-octagon-pentagon (5−8−5) carbon rings are known to exist in graphene grain boundaries. However, there are few systematic experimental studies on the formation, structure and distribution of periodic grain boundaries in graphene. Herein, scanning tunneling microscopy (STM) was applied to study periodic grain boundaries in monolayer graphene grown on a weakly interacting Cu(111) crystal. The periodic grain boundaries are formed after the thermal reconstruction of aperiodic boundaries, their structures agree well with the prediction of the coincident-site-lattice (CSL) theory. Periodic grain boundaries in quasi-freestanding graphene give sharp local density of states (LDOS) peaks in the tunneling spectra as opposed to the broad peaks of the aperiodic boundaries. This suggests that grain boundaries with high structural quality can introduce well-defined electronic states in graphene and modify its electronic properties.

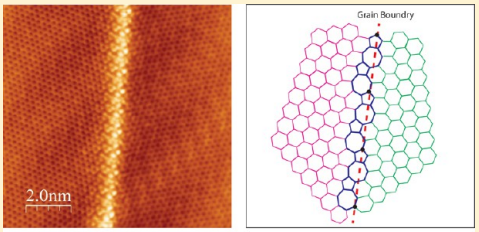

5-7-5-7 Periodic Grain Boundary

INTRODUCTION

Grain boundaries (GBs) in graphene have attracted much research interest recently, because they affect the mechanical, electrical, and chemical properties of the host material.[1−3] Transmission electron microscopy (TEM) studies[4−6] have revealed that the graphene grains are stitched together by nonhexagonal carbon rings such as pentagons and heptagons. Pentagons are paired with heptagons or octagons to form dislocation cores to reduce the strain in the graphene membrane.[7,8] Depending on whether dislocation cores are arranged in a periodic manner, GBs can be classified as periodic and aperiodic. Whereas aperiodic GBs act as electron scattering centers and degrade the electrical conductivity of graphene,[2,9] periodic GBs are predicted to have peculiar properties such as high mechanical strength,[10,11] magnetism,[12,13] and the presence of a well-defined transport gap.[14] The controlled formation of periodic GBs can be useful in tailoring the material properties and constructing graphene-based nanoscale devices. However, the ability to produce periodic GBs in graphene remains an experimental challenge. Apart from the recently reported 5−8−5 periodic GBs in graphene grown on nickel[15] and the GB loop in graphene grown on SiC(0001),[16] most experimentally observed GBs in graphene are meandering and aperiodic.[17−24]

GBs in graphene can be geometrically constructed from the connection of two displaced half-lattices by adding carbon atoms to fill the gap or subtracting carbon atoms to prevent overlap.[25] The domain orientation in polycrystalline graphene is strongly affected by the substrate. For example, the formation of 5−8−5 periodic GBs in Ni(111) is governed by the graphene−substrate interaction. The 5−8−5 periodic GBs come from the parallel translation of two graphene domains, with unit cell vectors $\mathbf{a}_1$ and $\mathbf{a}_2$, by the Burgers vector $\mathbf{b} = {}^1/_3(\mathbf{a}_1 + \mathbf{a}_2)$.[15] The strong interaction and close epitaxial relationship[26] between graphene and Ni(111) are crucial for such a domain displacement to occur spontaneously during graphene growth. However, the strong interaction also renders other types of domain displacements energetically unfavorable, which makes the formation of other periodic GBs highly unlikely.[15] Recently, GB migration and reconstruction induced by electron beam irradiation was observed by Kurasch et al. in freestanding graphene using high-resolution transmission electron microscopy (HRTEM).[5] An interesting question arises regarding the type of GBs that will appear if the graphene is grown and annealed on a weakly interacting substrate such as copper. To this end, we carried out systematic scanning tunneling microscopy (STM) studies to gain atomic insight into the formation of periodic grain boundaries on Cu(111) with a view toward understanding the electronic properties of decoupled GBs.

EXPERIMENTAL SECTION

Sample Preparation. The experiments were performed in an ultrahigh-vacuum (UHV) chamber with a base pressure of 8×10^{-11} mbar. A UHV STM unit (SPECS high-temperature STM 150 Aarhus) was used for imaging and spectroscopy studies. The Cu(111) surface (MaTeck GmbH) was cleaned by repeated argon-ion sputtering at $p(\mathrm{Ar}) = 1 \times 10^{-5}$ mbar and 1.5 keV, followed by annealing in the preparation chamber (base pressure = 1×10^{-9} mbar) at ∼600 °C. Coronene molecules were evaporated at 130 °C for 15 min (for the growth of graphene films) or 8 min (for the growth of graphene

Received: June 5, 2014
Published: August 1, 2014

   dx.doi.org/10.1021/ja5054847 | J. Am. Chem. Soc. 2014, 136, 12041−12046

islands) onto the clean Cu(111) surface with Knudsen cells (MBE-Komponenten GmbH). Subsequently, the substrate was annealed at ~600 °C for 15 min to grow graphene. The as-grown sample was annealed at ~600 °C for thermal reconstruction. After growth or annealing, the sample was characterized by STM in the main chamber at ~20 °C.

Oxygen Intercalation. Oxygen was leaked into the preparation chamber in the pressure range of 1×10^{-7} mbar. A copper substrate that had been pregrown with graphene islands was heated at 100 °C for 1 h to facilitate oxygen diffusion at the interface between graphene and copper.

Scanning Tunneling Spectroscopy (STS) Measurements. To rule out any contribution from tip artifacts, the STM tip was cleaned by repeated argon-ion sputtering. The tip was stabilized on the surface at −0.8 V and 300 pA. The bias was swept from −0.8 to 0.8 V, and the current was recorded. Numerical derivation with Gaussian filtering was used to obtain the dI/dV spectra. Twenty measurements were made to give the average dI/dV value at each measurement spot.

RESULTS AND DISCUSSION

Grain Boundary Evolution in Graphene on Cu(111). In this study, graphene films were prepared on Cu(111) single crystals by thermal decomposition of hydrocarbon molecules under UHV. A relatively low growth temperature of ~600 °C was applied to suppress copper evaporation and increase graphene nucleation density. This procedure created a mosaic film with a high density of meandering GBs (Figure 1a). Our intention was to investigate whether careful thermal annealing allows the GBs to be reconstructed into periodic structures.[27] Our STM investigation revealed that the density of GBs decreased and the average length increased with increasing annealing time (Figure 1a–c) in these polycrystalline graphene films. This can be explained by the Ostwald ripening of the graphene grains facilitated by dislocation migration,[5] that is, the growth of large grains up to a few hundred nanometers accompanied by the shrinkage of small grains. The activation energy for dislocation migration in freestanding graphene is about 5–6 eV.[28] However, the copper substrate acts as a catalyst to reduce the activation barrier[29] significantly, so that GB reconstruction by dislocation migration can occur at a relatively low temperature. This suggests that postgrowth annealing can be applied to improve the quality of small-grain-size polycrystalline graphene. Most of the GBs observed in our experiments were curved and aperiodic (Figure 1d). However, thermal annealing increased the probability of observing GBs with a locally straight section (Figure 1c). The GB straightening process seen here might have the same origin as that reported previously by Kurasch et al.,[5] as GBs in graphene are structurally fluid during the annealing process. The straight segments had lengths typically ranging from 10 to 50 nm. Atomic-resolution STM images revealed that these straight segments consisted of periodic corrugations localized in the boundary region (inset of Figure 1c). Herein, we assign them as periodic GBs. More STM images of periodic GBs can be found in Figure S1 (Supporting Information).

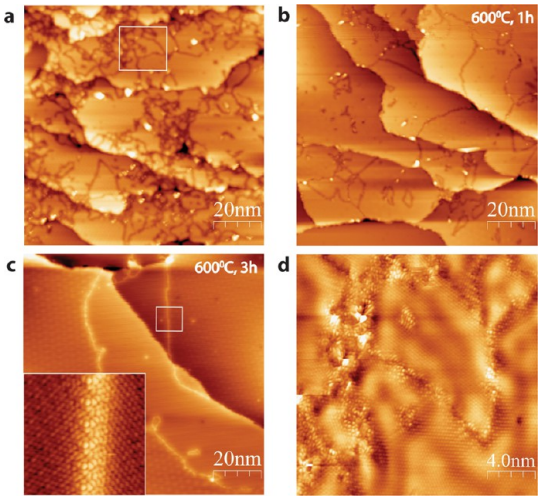

Figure 1. Effect of thermal annealing on the morphology of grain boundaries (GBs) in polycrystalline graphene films. (a–c) STM images of (a) as-grown graphene film on Cu(111) (−2 V, 300 pA; GBs shown as dark lines) (b) graphene film after annealing at ~600 °C for 1 h (GBs shown as dark lines), (c) graphene film after annealing at ~600 °C for 3 h (GBs shown as bright lines). Inset: High-resolution STM image (−5mV, 800pA) of the area marked in panel c, showing a straight and periodic GB in graphene. (d) High-resolution STM image (−20 mV, 1.5 nA) of the area marked in panel a, showing curved and aperiodic GBs in graphene. The morphology evolution of GBs under thermal annealing at 700 °C can be found in Figure S2 (Supporting Information).

Structural Characterization of Periodic Grain Boundaries in Graphene. Periodic GBs can be described by the periodicity d of the grain-boundary superlattice and the misorientation angle θ of the two domains. An STM height profile along the periodic corrugations gives the value of d. The misorientation angle θ is determined from the fast Fourier

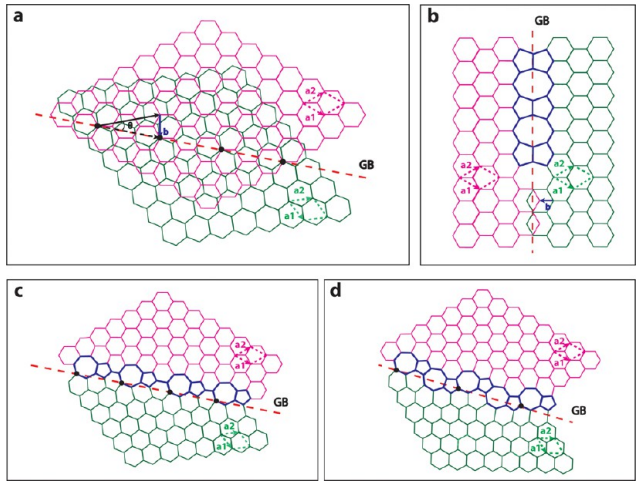

Figure 2. Schematic construction of periodic GBs in graphene based on the coincidence site lattice (CSL) theory. (a) Two superimposed graphene lattices, with unit cell vectors $\mathbf{a}_1$ and $\mathbf{a}_2$ (shown as dashed arrows), are rotated with respect to each other by the vector $\mathbf{b}$ (shown as a solid arrow in blue). θ denotes the corresponding misorientation angle between these two lattices. At certain misorientation angles, the two lattices have shared lattice points with a regular periodicity (shown as black dots). A periodic GB is formed along a line (dashed line in red) passing through these shared lattice points. (b) 5–8–5 periodic GB formed by translating two half-lattices by the vector $\mathbf{b} = {}^1/_3(\mathbf{a}_1 + \mathbf{a}_2)$ along the $\mathbf{a}_1-\mathbf{a}_2$ direction. Dislocation cores formed by pentagon–octagon–pentagon carbon rings are highlighted in blue. This structure has the highest density of coincident lattice points. (c) 5–7 periodic GB formed by rotating two half-lattices by 21.8°. Dislocation cores formed by pentagon–heptagon carbon rings are highlighted in blue. (d) 5–7–5–7 periodic GB formed by rotating two half-lattices by 32.2°. Dislocation cores formed by pairs of pentagon–heptagon carbon rings are highlighted in blue.

dx.doi.org/10.1021/ja5054847 | J. Am. Chem. Soc. 2014, 136, 12041–12046

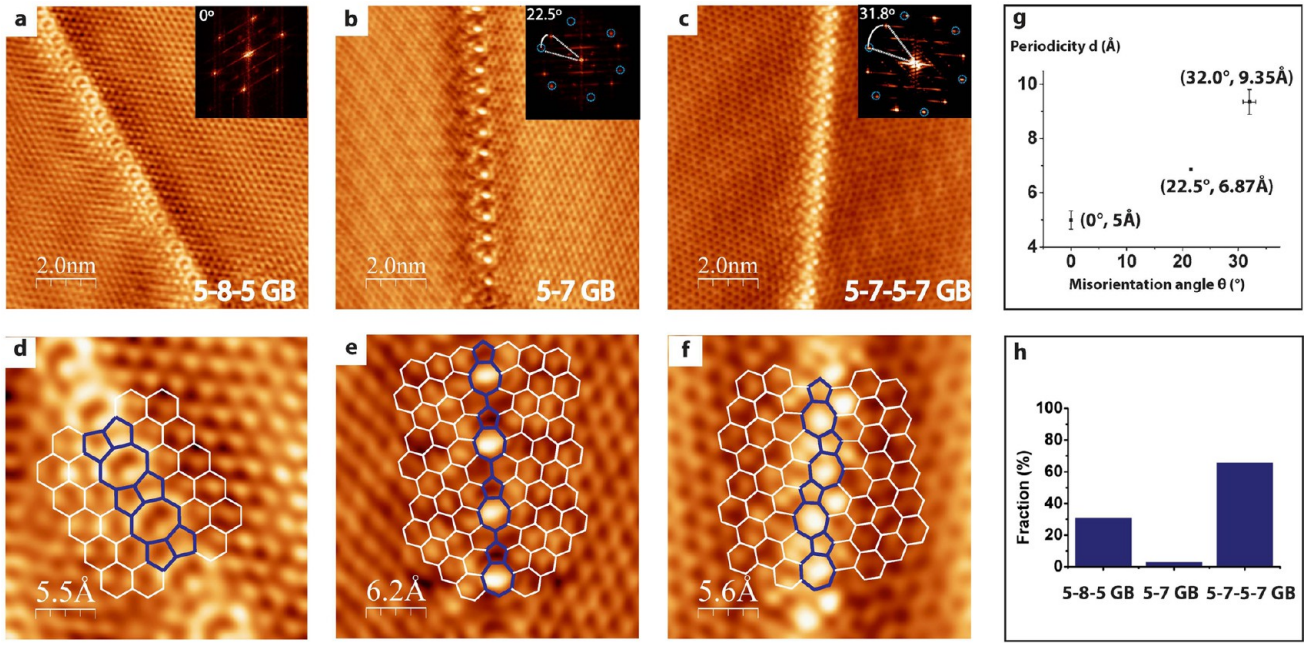

Figure 3. Structural characterization of periodic GBs in graphene. (a) High-resolution STM image of the 5−8−5 periodic GB (3 mV, 1.5 nA). (Inset: FFT showing the domain misorientation angle at 0°.) (b) High-resolution STM image of the 5−7 periodic GB (−20 mV, 500 pA). (Inset: FFT showing the domain misorientation angle at 22.5°.) (c) High-resolution STM image of the 5−7−5−7 periodic GB (−1 V, 400 pA). (Inset: FFT showing the domain misorientation angle at 31.8°.) (d−f) Magnified views of periodic GBs in panels a−c, respectively with the structural models superimposed. (g) Average values of the periodicity and misorientation angle of the three types of periodic GBs observed in our experiments. (h) Relative abundances of the three types of periodic GBs observed in our experiments.

transform (FFT) spectra of the high-resolution images. Two misoriented graphene domains produce two sets of spots in the FFT spectra, and their relative angle corresponds to the domain misorientation angle. By comparing the values of d and θ, we found that all of the periodic GBs observed in our experiments belonged to three distinct configurations. Graphene couples only weakly to Cu(111); hence, it is unlikely for preferential configurations to originate from the graphene−substrate registry. We found that the observed preference can be rationalized by the coincidence site lattice (CSL) theory proposed by Fasolino and co-workers.[30]

The CSL theory assumes that energetically favorable GBs must have a smooth connection between two grains. Such grain boundaries can be constructed according to the procedures illustrated in Figure 2a.

Based on this method, the GBs shown schematically in Figure 2b−d have higher density of coincidence lattice sites along the boundary compared to any other possible periodic GB structures (see ref 27 for detailed analysis). Qualitatively, one can consider these three structures as the energetically favorable configurations for periodic GBs in graphene. The calculated GB periodicity is 4.92 Å and the domain misorientation is 0° for the structure in Figure 2b. Similarly, the structure in Figure 2c has a calculated periodicity of 6.51 Å and a misorientation angle of 21.8°. The structure in Figure 2d has a periodicity of 8.87 Å and a misorientation angle of 32.2°.

Representative STM images of the three types of periodic GBs observed in our experiments are shown in panels a−c of Figure 3, with domain misorientation angles of 0°, 22.5°, and 31.8°, respectively (insets of Figure 3a−c). The average values of periodicity and misorientation angle for the three types of periodic grain boundaries are plotted in Figure 3g. The average values were found to match well with the structural models predicted by CSL theory. The small deviation between the calculated and measured values might come from STM image distortion or strain-related GB structure relaxation. This suggests that the favorable periodic GB configurations observed in our experiments are likely to come from the intrinsic thermodynamic stability of the GBs in graphene. Similar predictions based on DFT calculations were reported in recent theoretical papers.[7,30,31]

The proposed structural models (Figure 2b−d) of periodic GBs are superimposed on the STM images in Figure 3d−f. The periodic GB in Figure 3a is the previously reported 5−8−5 GB.[15] The repeating structural unit for the GB in Figure 3b is the 5−7 carbon rings. Therefore, we denote it as the 5−7 periodic GB. A structure similar to this 5−7 periodic GB was reported in an STM study of highly oriented pyrolytic graphite (HOPG).[32] Such boundaries are highly transparent to charge carriers in graphene, according to the theoretical calculations by Yazyev and Louie.[14] Based on the repeating structural units, the GB in Figure 3c can be denoted as the 5−7−5−7 periodic GB. The 5−7−5−7 GB has been predicted to have mechanical strength close to that of pristine graphene, which is highest among all GB structures.[10,11] As far as we know, this is the first time the presence of the 5−7−5−7 periodic GB in graphene has been experimentally observed. The relative abundance of periodic GBs is plotted in Figure 3h, suggesting that there exists a strong preference for the 5−7−5−7 GB. Theoretical studies have predicted a lower formation energy for the 5−7−5−7 GB compared to the 5−7 GB.[30,31] This result implies that the mechanical strength of the graphene film can be tuned by controlling the density of the mechanically stable 5−7−5−7 GBs.

We also found that short periodic GB segments can be joined together in a zigzag manner to form long faceted GBs (Figure 4). The faceting of GBs can also be rationalized by the coincident site lattice (CSL) theory. According to the CSL

dx.doi.org/10.1021/ja5054847 | J. Am. Chem. Soc. 2014, 136, 12041−12046

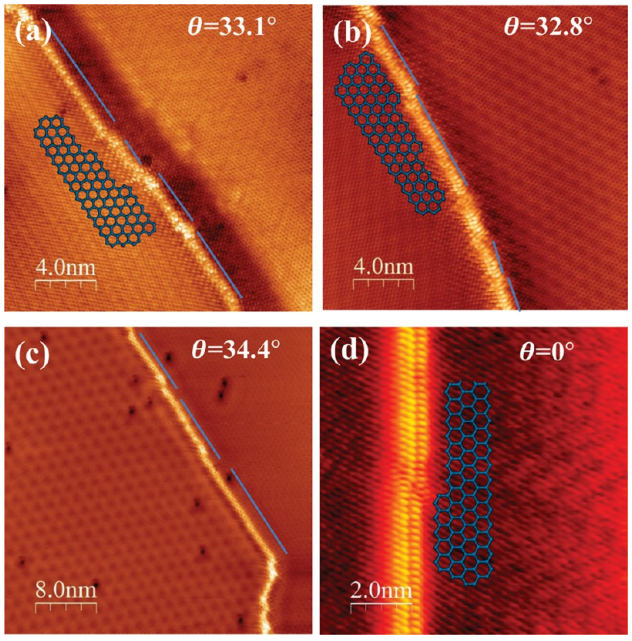

Figure 4. Representative STM images of faceted periodic GBs in graphene. Atomic-resolution STM images of (a–c) faceted 5–7–5–7 periodic GBs (V = −20 mV, I = 1 nA) and (d) faceted 5–8–5 periodic GBs (V = −6 mV, I = 600 pA).

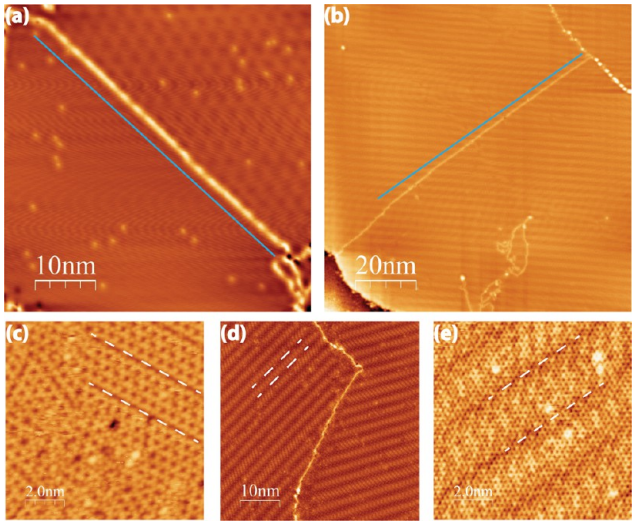

Figure 5. (a) STM image of a straight GB of ∼50-nm length after annealing of graphene islands on Cu(111) at 600 °C for 3 h (V = −2 V, I = 200 pA). (b) STM image of a ∼100-nm-long faceted grain boundary, prepared under conditions similar to those used fro panel a (V = −1.8 V, I = 200 pA). (c–e) STM images of stripe patterns on the substrate and under a graphene domain after oxygen adsorption on Cu(111). The stripe patterns are highlighted by dashed lines in white. (c) Atomic-resolution STM image (−400 mV, 500 pA) of the striped oxide superlattice on copper surface. (d) STM image (−1 V, 400 pA) of one graphene island. The underlying oxide stripe pattern is clearly adopted by graphene. (e) Atomic-resolution STM image (−500 mV, 400 pA) of the graphene island in panel d, showing both the stripe pattern and the hexagonal graphene lattice.

theory, GBs with a high density of coincident lattice points occur at certain values of the domain misorientation angle. The resulting GBs can be termed CSL boundaries. When the misorientation angle of two graphene domains deviates only slightly from the optimum values, there is a tendency for this GB to adopt the structure of the low-energy CSL GB. The mismatch in the values of the misorientation angle between this GB and the CSL GB is compensated by the formation of kinked sites. Through this reconstruction, the overall formation energy of the faceted GB is lowered.[33] A recent theoretical study also demonstrated that the length of the periodic segment depends on the deviation angle of the existing GB with respect to the optimum low-energy GB, with a larger deviation angle leading to a shorter periodic length.[34]

As shown in Figure 5, the longest straight GB observed in this work, within the scanning range of our STM, was about 50 nm (Figure 5a), and the longest faceted GB was about 100 nm (Figure 5b).

Electronic Properties of Grain Boundaries Studied by STS. We also explored the electronic structure of GBs using STS. We are well aware that the STS spectra of graphene are complicated by the substrate effect. The STS spectrum recorded at a perfect graphene domain shows a dip at around −0.6 eV corresponding to the shifted Dirac point due to metal doping.[35,36] Compared to the STS spectrum at a graphene domain, the STS spectrum in a GB region shows a similar dip at around −0.6 eV and enhanced tunneling conductance in the positive bias range. However, no distinct local density of states (LDOS) peaks could be resolved for the GBs, possibly owing to the LDOS convolution between graphene and Cu(111) (see Figure S3, Supporting Information).

To obtain quasifreestanding characteristics for graphene and its GBs, we employed the method of reactive oxygen intercalation to delaminate graphene from the metal substrate.[37,38] It has been reported that oxygen atoms form well-ordered stripe patterns on the bare Cu surface, giving rise to a "44" superstructure[39] (Figure 5c). Following the intercalation of oxygen between the graphene islands and the copper substrate, a similar stripelike pattern was observed on the graphene islands that was due to the underlying oxygen superstructure (Figure 5d,e). This indicates successful intercalation and decoupling of the graphene layer from the copper substrate. The intercalation efficiency was relatively high for polycrystalline graphene islands. The representative STM images of GBs before and after the intercalation are shown in Figure 6a–c.

After oxygen intercalation of polycrystalline graphene islands, STS was applied to probe the electronic structure of the 5–8–5 and 5–7–5–7 types of periodic GBs. dI/dV measurements were recorded at five spots (1–5) across the 5–8–5 (Figure 6d) and 5–7–5–7 (Figure 6e) GBs and compared with the spectra of the aperiodic GBs (Figure 6f). For all three types of GBs measured, parabolic LDOS curves with only one primary dip near the Fermi level were recorded at spots far from the boundary region (spots 1 and 5 in Figure 6d–f). We postulate that the interfacial oxygen acts as a buffer layer to suppress the doping of graphene by copper.

In the dI/dV spectra recorded in the GB region (spot 3 in Figure 6d–f), additional LDOS peaks can be seen. There are two peaks at about −0.4 and 0.16 eV for the 5–8–5 periodic GB (Figure 6d). The amplitude of these LDOS peaks decays as the tip is moved away from the GB. Such LDOS peaks can be explained by the localized electronic states induced by defects breaking the electron–hole symmetry in graphene lattice.[40] A previous DFT simulation study on the 5–8–5 periodic GB reported the occurrence of a sublattice-specific DOS.[41] A sharp peak at the Dirac point was observed for atoms belonging to

dx.doi.org/10.1021/ja5054847 | J. Am. Chem. Soc. 2014, 136, 12041–12046

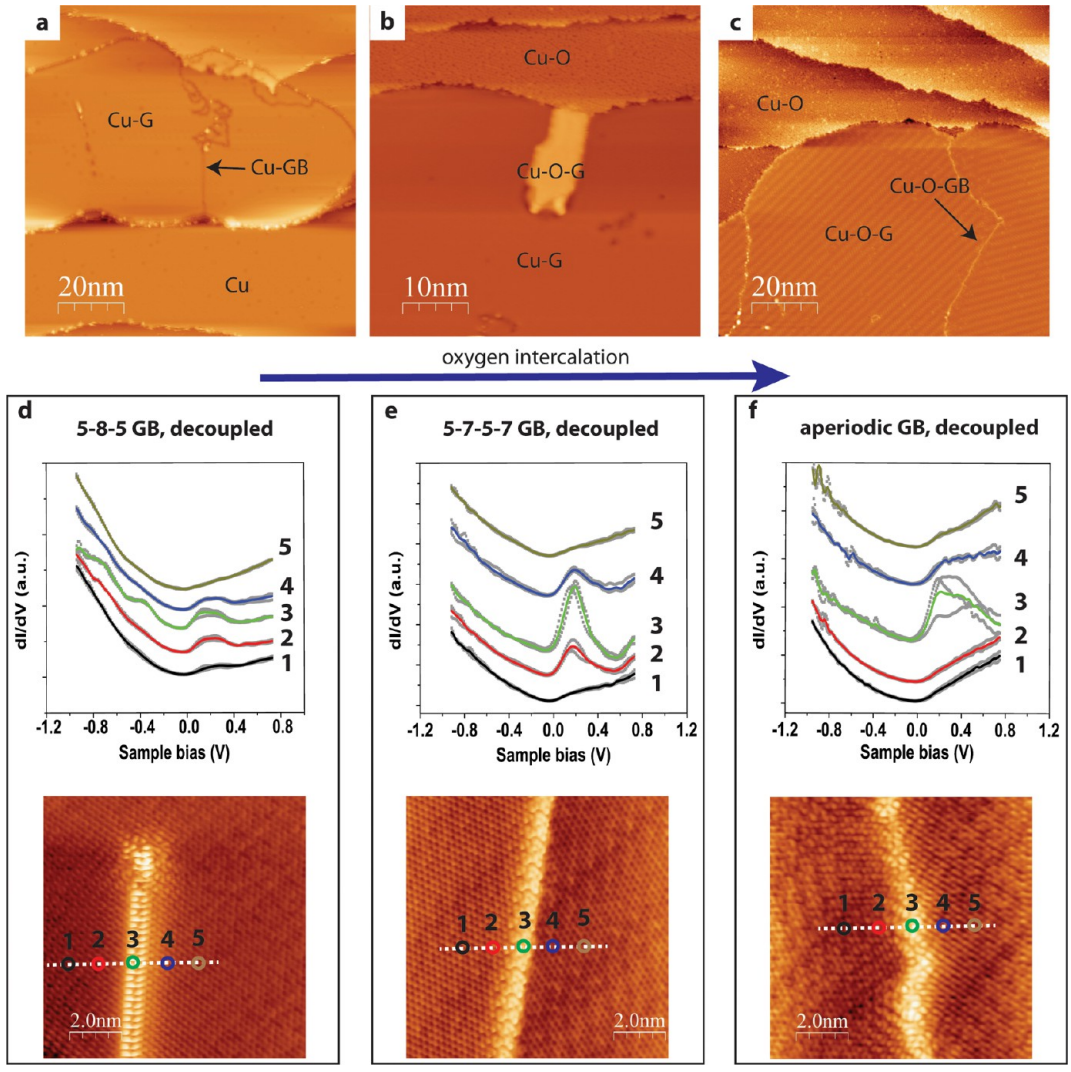

Figure 6. Electronic properties of periodic GBs in graphene. (a) STM image (−2 V, 300 pA) of graphene islands on Cu(111) before oxygen intercalation. (b) STM image (−1 V, 300 pA) of a partially intercalated graphene island on Cu(111). (c) STM image (−1 V, 300 pA) of a fully intercalated graphene island on Cu(111), showing well-ordered stripes on both the Cu surface and the graphene island. These stripes come from the superstructure of oxygen adsorbed on the Cu surface. This indicates that graphene is decoupled from the Cu(111) crystal by an oxygen buffer layer. (d) dI/dV spectra collected at five spots across a 5−8−5 periodic GB. (e) dI/dV spectra collected at five spots across a 5−7−5−7 periodic GB. (f) dI/dV spectra collected at five spots across an aperiodic GB.

one sublattice, whereas two peaks within 1 eV above and below the Dirac point can be attributed to another sublattice. Our measurements (Figure 6d) agree qualitatively with the DFT observation of the two states above and below the Dirac point, but the sharp peak at Dirac point was not observed. It was interesting to observe a sharp LDOS peak at 0.18 eV in the spectra taken at the vicinity of the 5−7−5−7 GB (Figure 6e). We compared the LDOS of the 5−7−5−7 GB to that of the aperiodic GB in Figure 6f. DFT simulations revealed van Hove singularities within 0.5 eV from the Dirac point.[31] Our measurements revealed a peak that can be correlated to the calculated empty state at about 0.2 eV; however, the theoretically predicted filled state was not observed. Examining the calculated density of states, we found that the empty state was indeed more intense than the filled state. The weaker filled state might be harder to observe because of thermal broadening in our room-temperature STS measurements. In contrast to the sharp LDOS peak of the 5−7−5−7 GB, the dI/dV curve of the aperiodic GB has a broad peak spanning the Fermi level to about 0.8 eV. For aperiodic GBs, random defects will induce localized electronic states with a broad energy distribution. This implies that GBs with high structural quality can introduce well-defined states to modify the electronic properties of graphene. A recent low-temperature STS measurement reported the observation of van Hove singularities in ordered GBs in graphene.[42]

■ CONCLUSIONS

Our results show that thermally annealing a mosaic polycrystalline graphene film grown on a metal surface allows the GBs to reconstruct and decrease in density and that nanometer-scale periodic GBs can be formed as a thermodynamically stable product. These results have implications for implementing a postgrowth annealing process to allow as-deposited graphene films to reconstruct to higher crystalline quality. Although the orientation of these periodic GBs is random on a macroscopic scale, our results raise the interesting question of whether the lithographical patterning of long gaps on graphene grown on

dx.doi.org/10.1021/ja5054847 | J. Am. Chem. Soc. 2014, 136, 12041−12046

metal provides a template for growing long, periodic GBs, where the gaps can be in-filled by regrown graphene strips. A postgrowth annealing process similar to what was applied here might allow for the reconstruction of the GBs at the stitched interfaces, leading to long sections of periodic GBs. If this can be achieved, the engineering of conducting circuits on graphene can be realized.

■ ASSOCIATED CONTENT

Supporting Information

Additional STM and STS characterization data. This material is available free of charge via the Internet at http://pubs.acs.org.

■ AUTHOR INFORMATION

Corresponding Author

E-mail: chmlohkp@nus.edu.sg

Notes

The authors declare no competing financial interest.

■ ACKNOWLEDGMENTS

K.P.L. acknowledges funding support from NRF-CRP Grant "Fundamental Limits and Applications of the Atomic Level Ion Source (Angstrom Level Imaging and Quantum Foundry)" and MOE Tier 2 "From in-situ observation to the growth scaling of graphene quantum dots" R-143-000-493-112. The authors thank Dr. Zheng Yi for helpful discussions.

■ REFERENCES

(1) Tsen, A. W.; Brown, L.; Levendorf, M. P.; Ghahari, F.; Huang, P. Y.; Havener, R. W.; Ruiz-Vargas, C. S.; Muller, D. A.; Kim, P.; Park, J. *Science* **2012**, *336*, 1143.

(2) Yu, Q.; Jauregui, L. A.; Wu, W.; Colby, R.; Tian, J.; Su, Z.; Cao, H.; Liu, Z.; Pandey, D.; Wei, D.; Chung, T. F.; Peng, P.; Guisinger, N. P.; Stach, E. A.; Bao, J.; Pei, S.-S.; Chen, Y. P. *Nat. Mater.* **2011**, *10*, 443.

(3) Lee, G.-H.; Cooper, R. C.; An, S. J.; Lee, S.; van der Zande, A.; Petrone, N.; Hammerberg, A. G.; Lee, C.; Crawford, B.; Oliver, W.; Kysar, J. W.; Hone, J. *Science* **2013**, *340*, 1073.

(4) Huang, P. Y.; Ruiz-Vargas, C. S.; van der Zande, A. M.; Whitney, W. S.; Levendorf, M. P.; Kevek, J. W.; Garg, S.; Alden, J. S.; Hustedt, C. J.; Zhu, Y.; Park, J.; McEuen, P. L.; Muller, D. A. *Nature* **2011**, *469*, 389.

(5) Kurasch, S.; Kotakoski, J.; Lehtinen, O.; Skákalová, V.; Smet, J.; Krill, C. E.; Krasheninnikov, A. V.; Kaiser, U. *Nano Lett.* **2012**, *12*, 3168.

(6) Kim, K.; Lee, Z.; Regan, W.; Kisielowski, C.; Crommie, M. F.; Zettl, A. *ACS Nano* **2011**, *5*, 2142.

(7) Liu, Y.; Yakobson, B. I. *Nano Lett.* **2010**, *10*, 2178.

(8) Yakobson, B. I.; Ding, F. *ACS Nano* **2011**, *5*, 1569.

(9) Tapasztó, L.; Nemes-Incze, P.; Dobrik, G.; Jae Yoo, K.; Hwang, C.; Biró, L. P. *Appl. Phys. Lett.* **2012**, *100*, 053114.

(10) Grantab, R.; Shenoy, V. B.; Ruoff, R. S. *Science* **2010**, *330*, 946.

(11) Wei, Y.; Wu, J.; Yin, H.; Shi, X.; Yang, R.; Dresselhaus, M. *Nat. Mater.* **2012**, *11*, 759.

(12) Kou, L.; Tang, C.; Guo, W.; Chen, C. *ACS Nano* **2011**, *5*, 1012.

(13) López-Sancho, M. P.; de Juan, F.; Vozmediano, M. A. H. *Phys. Rev. B* **2009**, *79*, 075413.

(14) Yazyev, O. V.; Louie, S. G. *Nat. Mater.* **2010**, *9*, 806.

(15) Lahiri, J.; Lin, Y.; Bozkurt, P.; Oleynik, I. I.; Batzill, M. *Nat. Nano* **2010**, *5*, 326.

(16) Cockayne, E.; Rutter, G. M.; Guisinger, N. P.; Crain, J. N.; First, P. N.; Stroscio, J. A. *Phys. Rev. B* **2011**, *83*, 195425.

(17) László, P. B.; Philippe, L. *New J. Phys.* **2013**, *15*, 035024.

(18) Coraux, J.; N'Diaye, A. T.; Busse, C.; Michely, T. *Nano Lett.* **2008**, *8*, 565.

(19) Koepke, J. C.; Wood, J. D.; Estrada, D.; Ong, Z.-Y.; He, K. T.; Pop, E.; Lyding, J. W. *ACS Nano* **2012**, *7*, 75.

(20) Jacobson, P.; Stöger, B.; Garhofer, A.; Parkinson, G. S.; Schmid, M.; Caudillo, R.; Mittendorfer, F.; Redinger, J.; Diebold, U. *J. Phys. Chem. Lett.* **2011**, *3*, 136.

(21) Nemes-Incze, P.; Yoo, K. J.; Tapasztó, L.; Dobrik, G.; Lábár, J.; Horváth, Z. E.; Hwang, C.; Biró, L. P. *Appl. Phys. Lett.* **2011**, *99*, 023104.

(22) Nemes-Incze, P.; Vancsó, P.; Osváth, Z.; Márk, G. I.; Jin, X.; Kim, Y.-S.; Hwang, C.; Lambin, P.; Chapelier, C.; PéterBiró, L. *Carbon* **2013**, *64*, 178.

(23) Biedermann, L. B.; Bolen, M. L.; Capano, M. A.; Zemlyanov, D.; Reifenberger, R. G. *Phys. Rev. B* **2009**, *79*, 125411.

(24) Banhart, F.; Kotakoski, J.; Krasheninnikov, A. V. *ACS Nano* **2010**, *5*, 26.

(25) Kittel, C. *Introduction to Solid State Physics*, 8th ed.; Wiley: New York, 2005.

(26) Jacobson, P.; Stöger, B.; Garhofer, A.; Parkinson, G. S.; Schmid, M.; Caudillo, R.; Mittendorfer, F.; Redinger, J.; Diebold, U. *ACS Nano* **2012**, *6*, 3564.

(27) Cho, J.; Gao, L.; Tian, J.; Cao, H.; Wu, W.; Yu, Q.; Yitamben, E. N.; Fisher, B.; Guest, J. R.; Chen, Y. P.; Guisinger, N. P. *ACS Nano* **2011**, *5*, 3607.

(28) Kotakoski, J.; Krasheninnikov, A. V.; Kaiser, U.; Meyer, J. C. *Phys. Rev. Lett.* **2011**, *106*, 105505.

(29) Meng, L.; Jiang, J.; Wang, J.; Ding, F. *J. Phys. Chem. C* **2013**, *118*, 720.

(30) Carlsson, J. M.; Ghiringhelli, L. M.; Fasolino, A. *Phys. Rev. B* **2011**, *84*, 165423.

(31) Yazyev, O. V.; Louie, S. G. *Phys. Rev. B* **2010**, *81*, 195420.

(32) Simonis, P.; Goffaux, C.; Thiry, P. A.; Biro, L. P.; Lambin, P.; Meunier, V. *Surf. Sci.* **2002**, *511*, 319.

(33) Priester, L. *Grain Boundaries: From Theory to Engineering*; Springer: New York, 2012; Vol. *172*.

(34) Zhang, Z.; Yang, Y.; Yakobson, B. I. *J. Mech. Phys. Solids* **2014**, *70*, 62.

(35) Gao, L.; Guest, J. R.; Guisinger, N. P. *Nano Lett.* **2010**, *10*, 3512.

(36) Walter, A. L.; Nie, S.; Bostwick, A.; Kim, K. S.; Moreschini, L.; Chang, Y. J.; Innocenti, D.; Horn, K.; McCarty, K. F.; Rotenberg, E. *Phys. Rev. B* **2011**, *84*, 195443.

(37) Sutter, P.; Sadowski, J. T.; Sutter, E. A. *J. Am. Chem. Soc.* **2010**, *132*, 8175.

(38) Lu, J.; Zhang, K.; Feng Liu, X.; Zhang, H.; Chien Sum, T.; Castro Neto, A. H.; Loh, K. P. *Nat. Commun.* **2013**, *4*, 2681.

(39) Matsumoto, T.; Bennett, R. A.; Stone, P.; Yamada, T.; Domen, K.; Bowker, M. *Surf. Sci.* **2001**, *471*, 225.

(40) Castro Neto, A. H.; Guinea, F.; Peres, N. M. R.; Novoselov, K. S.; Geim, A. K. *Rev. Mod. Phys.* **2009**, *81*, 109.

(41) Vancsó, P.; Márk, G. I.; Lambin, P.; Mayer, A.; Kim, Y.-S.; Hwang, C.; Biró, L. P. *Carbon* **2013**, *64*, 101.

(42) Ma, C.; Sun, H.; Zhao, Y.; Li, B.; Li, Q.; Zhao, A.; Wang, X.; Luo, Y.; Yang, J.; Wang, B.; Hou, J. G. *Phys. Rev. Lett.* **2014**, *112*, 226802.